

Published in final edited form as:

Biochemistry. 2010 September 28; 49(38): 8434–8441. doi:10.1021/bi1007595.

Comparative kinetics of cofactor association and dissociation for the human and trypanosomal S-adenosylhomocysteine hydrolases. 3. The role of lysyl and tyrosyl residues of the C-terminal extension†

Sumin Cai[‡], Jianwen Fang^{*§}, Qing-Shan Li^{||}, Ronald T. Borchardt^{||}, Krzysztof Kuczera^{‡,⊥}, C. Russell Middaugh^{||}, and Richard L. Schowen^{‡,||,⊥}

Departments of Molecular Biosciences, Pharmaceutical Chemistry, Chemistry, and the Applied Bioinformatics Laboratory, the University of Kansas, Lawrence, Kansas 66047

Abstract

Based on the available X-ray structures of S-adenosylhomocysteine hydrolases (SAHHs), free energy simulations employing the MM-GBSA approach were applied to predict residues important to the differential cofactor binding properties of human and trypanosomal SAHHs (Hs-SAHH and Tc-SAHH), within 5 Å of the cofactor NAD⁺/NADH binding site. Among the 38 residues in this region, only four are different between the two enzymes. Surprisingly, the four non-identical residues make no major contribution to differential cofactor binding between Hs-SAHH and Tc-SAHH. On the other hand, four pairs of *identical* residues are shown by free energy simulations to differentiate cofactor binding between Hs-SAHH and Tc-SAHH. Experimental mutagenesis was performed to test these predictions for a lysine residue and a tyrosine residue of the C-terminal extension that penetrates a partner subunit to form part of the cofactor binding site. The K431A mutant of Tc-SAHH (TcK431A) loses its cofactor binding affinity but retains the wild type's tetrameric structure, while the corresponding mutant of Hs-SAHH (HsK426A) loses both cofactor affinity and tetrameric structure (Ault-Riche et al., 1994 *J Biol Chem*, 269, 31472–8). The tyrosine mutants HsY430A and TcY435A alter the NAD⁺ association and dissociation kinetics, with HsY430A increasing the cofactor equilibrium dissociation constant from approximately 10 nM (Hs-SAHH) to about 800 nM while TcY435A increases the cofactor equilibrium dissociation constant from approximately 100 nM (Tc-SAHH) to about 1 mM. Both changes result from larger increases in off-rate combined with smaller decreases in on-rate. These investigations demonstrate that computational free energy decomposition may be used to guide experimental studies by suggesting sensitive sites for mutagenesis. Our finding that identical residues in two orthologous proteins may give significantly different binding free energy contributions strongly suggests that

†This study was supported by Grant GM-29332 from the National Institute of General Medical Sciences.

*To whom correspondence should be addressed: Jianwen Fang, Applied Bioinformatics Laboratory, 2034 Becker Dr., The University of Kansas, Lawrence KS 66047, Tel: +1-785-864-3349, FAX: +1-785-864-8141, jwfang@ku.edu.

‡Department of Molecular Biosciences

§Applied Bioinformatics Laboratory

||Department of Pharmaceutical Chemistry

⊥Department of Chemistry

Supporting Information Available.

Figure S1: The dependence of the concentrations of NAD⁺ on the rate constants for the slow-binding phase of the association of NAD⁺ with the apo-forms of mutant HY430A and wild type Hs-SAHHa at 23 °C and pH 7.4. Figure S2: The dependence of the concentrations of NAD⁺ on the rate constants for the slow-binding phase of the association of NAD⁺ with the apo-forms of mutant TcY435A and wt Tc-SAHH (the wt Tc-SAHH data will be presented in detail elsewhere) at 23 °C and pH 7.4. Figure S3: RMSD for the dynamic simulations of Hs-SAHH and Tc-SAHH. This material is available free of charge via the Internet at <http://pubs.acs.org>. Figure S4: RMSD for the predicted four identical residues that may give different binding free energy contributions in Hs-SAHH and Tc-SAHH.

comparative studies of homologous proteins should investigate not only different residues, but also identical residues in these proteins.

Keywords

S-adenosyl-L-homocysteine hydrolase; *Homo sapiens*; *Trypanosoma cruzi*; cofactor binding kinetics; free-energy simulations; computational alanine scan; C-terminal extensions

Mammals (1) and the protozoan parasites *Trypanosoma* (2), *Plasmodium* (3), and *Leishmania* (4) all have S-adenosyl-L-homocysteine hydrolases (SAHs), which catalyze the hydrolysis of S-adenosyl-L-homocysteine (AdoHcy) to adenosine (Ado) and L-homocysteine (Hcy). SAHs are metabolically important enzymes because AdoHcy is a feedback inhibitor of S-adenosylmethionine (AdoMet)-dependent transmethylation enzymes that play crucial roles in regulating methylation of a variety of macromolecules and small molecules (5). For this reason SAHs have been considered as possible anti-parasitic drug targets. The catalytic mechanism of SAHs includes a complete redox cycle of a nicotinamide cofactor (NAD⁺/NADH) that is tightly bound within the enzyme (1,6). The catalytic properties of human and parasitic SAHs are very similar. This discourages the design of anti-parasitic drugs as substrate analogs or mechanism-based inhibitors. Our studies of human SAH (Hs-SAHH) and trypanosomal SAH (Tc-SAHH), however, reveal significant differences in the kinetics and thermodynamics of nicotinamide cofactor binding between these two enzymes (7). This provides possible approaches to the design of inhibitors having differential effects on Tc-SAHH compared to Hs-SAHH. Such inhibitors may benefit patients who suffer from Chagas disease which is transmitted by the parasite *Trypanosoma cruzi* (8).

Several X-ray crystallographic structures of Hs-SAHH such as 1A7A (1) and 1LI4 (6) and Tc-SAHH (PDB: 1XBE, unpublished data of Drs. Q.-S. Li and W. Huang) are available. Both SAHs are homotetramers and each subunit contains a substrate-binding domain, a cofactor (NAD⁺/NADH)-binding domain and a C-terminal tail which covers the cofactor-binding site of the neighboring subunit (Figure 1). A lysine and a tyrosine located within the C-terminal chain are very close to the NAD(H) cofactor in the X-ray structures and may provide important contributions to cofactor binding of SAHs. Two main conformations of SAHH have been characterized: one is a ligand-free “open” form with the cofactor NAD⁺ bound (9) and the other is a “closed” form containing the cofactor NADH and oxidized substrate (DHCeA (1) or NepA (6)). The atomic-level mechanism of the differential nicotinamide cofactor binding properties of Hs-SAHH and Tc-SAHH, however, is not yet clear (7).

To analyze microscopic differences between NAD binding to Hs-SAHH and Tc-SAHH, we have estimated cofactor binding free energy decompositions based on the MM-GBSA approach (10). The free energy decomposition estimations permit the prediction of residues which significantly contribute the most to cofactor binding. In the present study, experimental mutagenesis was then performed to test computational predictions for two pairs of conserved residues: a lysine and a tyrosine in the C-terminal tail in both enzymes. For a majority of these mutants, the experimental results were qualitatively consistent with the computational predictions, confirming the utility of MM-GBSA free energy estimations for identification of functionally important protein sites.

Methods and Materials

Computational procedures

The starting crystallographic structures of Hs-SAHH and Tc-SAHH were downloaded from the Protein Data Bank (PDB) (entries 1A7A and 1XBE, respectively). Calculations for another crystal structure of Hs-SAHH (PDB code: 1IL4) yielded very similar results. Thus, only the data for the 1A7A structure are shown in this study. The 1A7A structure was originally solved by incorporating selenium atoms (SE) in place of the sulfurs in Met residues. Assuming that this does not influence structure, we replaced Se atoms with S atoms and renamed the residues from MSE to MET. The simulation system was set up using the Xleap module of the Amber 7 software package (<http://ambermd.org/>). The SAHH homotetramer is a “dimer of dimers”, with one of the dimers formed by subunits A and B, and the other formed by subunits C and D. In brief, the protein (the AB dimer - each subunit bound with one NADH and one inhibitor) was solvated using a periodic truncated octahedral box of 29,419 water molecules, as described by the TIP3P model (11), and extended to a distance of 10 Å from any solute atom. The system was then neutralized by 16 sodium cations initially placed around the protein using a Coulombic potential on a grid. All minimization and molecular dynamics (MD) were performed with the Amber 7 suite of programs. The ff99 force field was used for proteins and NADH cofactor throughout the energy minimization and MD simulations. The starting geometry of ligands was taken from the protein PDB files. The input files for ligand MD simulations were prepared with antechAmber program in Amber 7, which uses General Amber Force Field (GAFF). Partial charges on the ligand atoms were calculated with the AM1-BCC method available in antechAmber (12).

Energy Minimization—The energy minimization was performed using the sander module in the Amber 7 suite of programs with the particle - mesh Ewald method for inclusion of long-range electrostatic interactions (13). We used two stages of energy minimization. In the first stage, only water molecules were minimized while the protein was fixed. The second stage minimized the entire system. Each stage was conducted with 500 cycles of steepest descent followed by 4500 conjugate steps of gradient minimization. The non-bonded cutoff was set to 12.0 Å.

Molecular Dynamics Simulations—The equilibration process was carried out in two stages following the protocol suggested in the Amber 7 manual. In the first stage, the system was heated gradually from a low temperature of 100 K to 300 K over 10 picoseconds (ps) simulation time with a time step of 2 femtoseconds (fs). A cutoff distance of 12 Å was used for the non-bonded interaction. The SHAKE algorithm was used to constrain the bonds involving hydrogen atoms and the force evaluations for these bonds were omitted (14). A periodic boundary with a constant volume and without pressure control was used. Then a second 10 ps equilibration was continued under a constant pressure and a constant temperature with isotropic position scaling to adjust the density of water to experimental values. After that, the entire system was equilibrated for 100 ps under a constant temperature of 300 K and a constant pressure of 1 bar. The SHAKE algorithm and 2 fs time steps were employed through all MD stages.

A 500 ps production run was performed with the same protocol used in the final stage of equilibration. After the simulation was completed, the ptraj module in Amber 7 was used to re-image the whole trajectory (including all equilibration and production runs), and to remove the waters and Na⁺ from the trajectory file, and to calculate the root-mean-square deviations (rmsd) of backbone atoms from the starting structure over the entire course. Fifty snapshots were taken at 2-ps intervals from the section of the MD trajectory where the rmsd

reached a plateau and were used for further analysis. These sections corresponded to an rmsd of about 1.5 Å for Hs-SAHH and an rmsd of about 1.3 Å for Tc-SAHH.

Calculation of energy decomposition by MM-GBSA—The residue-level free energy contributions to the cofactor binding were estimated using the MM-GBPA approach implemented in the `mm_pbsa.pl` script available in the Amber package. MM-GBSA is a post-processing method that can be used to evaluate free energy contributions at the residue level of binding of molecules in solution (15). It combines the molecular mechanical energies with the implicit solvent approaches. The molecular mechanical energies, representing internal energy, Van der Waals and electrostatic interactions, are calculated using the `sander` program in the AMBER package. The generalized Born (GB) model implemented in `sander` is used to estimate the electrostatic contribution to the solvation free energy, and the solvent-accessible surface area dependent term is used to determine the hydrophobic contribution to the solvation energy. The conformational entropies could be estimated using normal mode analysis but were not considered because of computer resource limitations. The entropic term is probably much smaller than the others and may be neglected in comparative studies of very similar systems (10). In this study, we used the single trajectory protocol (10) based on the assumption that the snapshots of the protein and cofactor taken from the complex trajectory are similar to those that would emerge from separate trajectories of protein and cofactor, or that the differences in the snapshots of single and separate trajectories are consistent between Hs-SAHH and Tc-SAHH. Both circumstances are considered acceptable because we were interested in the relative difference of the free energy contributions in these residues in Tc-SAHH and Hs-SAHH.

The simulated complex was a dimer bound with two cofactors and inhibitors [closed-form Hs-SAHH with DHCeA (pdb code: 1A7A) and closed-form Tc-SAHH with NepA (pdb code: 1XBE)]. In the analysis of individual residue contributions to ΔG , we only considered the 38 residues within 5 Å of the NAD(H) binding site in Hs-SAHH as well as Tc-SAHH. We calculated the difference of free energy contributions of all of these residues.

Experimental procedures

Construction of the mutants of Hs-SAHH and Tc-SAHH—The wild type genes of Hs-SAHH and Tc-SAHH were each inserted into its own copy of the pPROK-1 vector (Clontech, CA). Three alanine mutants (HsY430A, TcK431A, TcY435A) were prepared by the site-directed mutagenesis PCR. The primer sequences are listed below:

HsY430A: 5'-- CAAGCCGGATCACGCCGCTACTGAGA -- 3'
 5' -- TCTCAGTAGCGGGCGTGATCCGGCTTG -- 3'
 TcK431A: 5' -- ACGGCCCATTCGCGCCGACCACTACC -- 3'
 5' -- GGTAGTGGTCCGGCGGAATGGGCCGT -- 3'
 TcY435A: 5' -- AAGCCGGACCACGCCGCTACTAATCG -- 3'
 5' -- CGATTAGTAGCGGGCGTGGTCCGGCTT -- 3'

The amplification reactions of HsY430A, TcK431A and TcY435A were performed in a volume of 50 μ L containing 20 ng template, 25 pmol of 5' and 3' primers, 12.5 nmol of each deoxynucleoside triphosphate, 3 U native Pfu DNA polymerase (Stratagene), 6 μ L 10x Pfu buffer and 2.5 μ L DMSO. The steps of the PCR program were set up as follows: 1) 92 °C for 4 min; 2) 25 cycles of 92 °C for 30 sec, 52 °C for 30 sec and 68 °C for 20 mins; 3) 68 °C for 10 min; 4) hold at 4 °C. The PCR products of HsY430A and TcK431A were purified with a Qiagen PCR purification kit, while the PCR product of TcY435A contains two fragments of different sizes. The correct-size band (large size) was cut and collected from a 1 % DNA gel (low melting point) and then the PCR product was recycled by a Qiagen gel

extraction kit. These three purified PCR products were digested by DpnI (Biolab) and transformed into *E. coli* competent cell stain JM109 (Sigma). The purified mutant genes were confirmed by DNA sequencing.

Purification of the mutants of Hs-SAHH and Tc-SAHH—The procedures of overexpression (7), purification (7) and cell-free extract preparation (16) of the Hs-SAHH and Tc-SAHH mutants were similar to those previously described for the wild type SAHHS with modifications as follows. The cell-free extracts were passed through a FPLC system (Amersham Biosciences) including four different columns, namely a Q-sepharose Fast Flow column (26/10), Hiload Phenyl-sepharose column (26/10), Hiload Superdex 200 (16/60) and MonoQ (10/10) column. Buffer A is 25 mM Tris-HCl buffer pH 7.4, 1 mM EDTA, 40 μ M NAD⁺. Buffer B is 80 mM Tris-HCl buffer pH 7.4, 1 mM EDTA, 1 M NaCl and 40 μ M NAD⁺. After the Q-sepharose Fast Flow column (26/10), mutant proteins were identified by SDS-PAGE. The mutant TcK431A was purified employing only by Q-sepharose Fast Flow column (26/10) and Hiload Superdex 200 (16/60) columns.

Hydrolytic activity assay—The procedures for measuring SAHH activity in the hydrolytic direction were as described in previous work (16). The generated Ado was quickly removed by Ado deaminase to drive completion of the hydrolytic reaction. The rate of Hcy production was coupled with the formation of TNB²⁻ from DTNB. TNB²⁻ is intensely yellow and was determined at the absorption wavelength of 412 nm by UV spectroscopy.

Reconstitution of the NAD⁺ form and NADH form of Hs-SAHH and Tc-SAHH mutants—Preparation of the apo forms of Hs-SAHH and Tc-SAHH mutants and reconstitution of the NAD⁺ and the NADH forms of Hs-SAHH and Tc-SAHH mutants followed the same procedures described previously for wild type SAHHS (16). Apo forms of SAHH mutants were prepared by using 80% (v/v) acid ammonium sulfate with 2–5 mM DTT to precipitate purified mutants three times (pH 2.92, pH 3.12 and pH 7.2). The proteins collected by centrifugation were dissolved in 50 mM phosphate buffer at pH 7.2 containing 1 mM EDTA. 1 mM NAD⁺ or NADH were incubated with 10 mg/mL apo forms of the SAHH mutants for 12 h at 4 °C. The reconstituted NAD⁺ (or NADH) form of the mutants was then purified by a Hiload Superdex 200 (16/60) column (Amersham Sciences).

Determination of contents of NADH in the isolated Hs-SAHH and Tc-SAHH mutants—The mutant proteins (395 μ g in 90 μ L of 50 mM phosphate buffer, pH 7.2, 1 mM EDTA) were mixed with 10 μ L of 1 M Na₂CO₃/NaHCO₃, pH 10.7. A volume of 700 μ L of 95 % ethanol was then added to denature proteins and release NADH into solution. After centrifugation at 13,400 rpm for 10 min to remove precipitated proteins, the fluorescence intensity of NADH was measured by a photon technologies QM-3 scanning luminescence spectrophotometer. The excitation wavelength was 340 nm and the emission wavelength was 450 nm. NADH standards were prepared ranging from 0.1–10 μ M and were used to determine NADH content. The NADH content of SAHH inactivated by NepA was used as a control (100 % NAD⁺ reduced to NADH).

Determination of contents of NAD⁺ in Hs-SAHH and Tc-SAHH mutants—The mutant proteins (395 μ g in 80 μ L of 50 mM KPBS, pH 7.2, 1 mM EDTA) were denatured by addition of 2 μ L of 5 M HClO₄. Samples were centrifuged at 13,400 rpm for 10 mins at 4 °C to remove precipitated proteins. Supernatant was injected into a reversed-phase C18 column (Vydac 218TP54, 300 Å, 5 μ m, 4.5×250 mm) to measure the concentration of NAD⁺ at 258 nm. The NAD⁺ standard curve was made for the range of 1–200 μ M. NAD⁺ was eluted from the HPLC column at ~ 5.9 min by a gradient of 2–10 % mobile phase B over 20 min

with a flow rate of 1 mL/min. Mobile phase A contained 10 mM 1-heptanesulfonic acid, 50 mM sodium phosphate, pH 3.2 while mobile phase B contained 80 % acetonitrile and 20 % 2-propanol.

Results

Computational Results

Single-residue contributions to the free energy of NADH binding to Hs-SAHH and Tc-SAHH—Hs-SAHH and Tc-SAHH share about 70 % identity of their amino-acid sequences. In superimposed structures of Hs-SAHH and Tc-SAHH, with the superposition centered on the center of mass of the cofactor NADH, there are 38 protein residues within a 5-Å thick shell around the cofactor. To identify protein residues with the largest contributions to differential cofactor binding of Hs-SAHH and Tc-SAHH, contributions to the NADH binding free energy from every residue within 5 Å of the cofactor binding site were calculated and the results are listed in Table 1. Thirty-four of these 38 residues (89 %) are identical in Hs-SAHH and Tc-SAHH, while four pairs are different. In most cases the individual residue contributions to cofactor binding are very similar in the two proteins. Interestingly, four pairs of identical residues (HsAaaTc: 191ASN193; 243GLU242; 426LYS431; 430TYR435), which are shown in red in Table 1, make significantly different free-energy contributions to the binding of NADH to Hs-SAHH and Tc-SAHH.

Experimental Results

Y430 in the C-terminal extension of Hs-SAHH may slightly influence binding of NAD⁺ and NADH to apo-Hs-SAHH—The mutant HsY430A is a purified protein of the correct molecular mass (190 kD) and possesses an intact tetrameric structure (as evaluated by size exclusion chromatography). The enzyme is isolated from the expression system with 30 ± 5 % active-site occupancy by NAD⁺ (HPLC) and 86 ± 5% active-site occupancy by NADH (fluorescence). Denaturation of the isolated enzyme yielded 3.1 ± 0.1% adenosine and 81 ± 1% adenine. Reconstitution of apo-HsY430A with NAD⁺ yielded protein with 79 ± 1% occupancy (HPLC) and 70 ± 1% catalytic activity. Reconstitution of apo-HsY430A with NADH yielded protein with 94 ± 1% occupancy (fluorescence).

K431 in the C-terminal extension of Tc-SAHH is required for the binding of NAD⁺ and NADH to apo-Tc-SAHH—The purified mutant TcK431A was also of the correct molecular mass (194 kDa) and possesses an intact tetrameric structure (size exclusion chromatography). The enzyme is isolated from the expression system with no NAD⁺ present (detection limit 0.1 % active-site occupancy) and little NADH occupancy (1.30 ± 0.03 % active-site occupancy by fluorescence). Attempts at reconstitution with cofactor of apo-TcK431A yielded no detectable occupancy by either NAD⁺ or NADH.

Y435 in the C-terminal extension of Tc-SAHH is required for tight binding of NAD⁺ and NADH to apo-Tc-SAHH—The mutant TcY435A was again of the correct molecular mass (194 kDa) and possesses an intact tetrameric structure (size exclusion chromatography). The enzyme is isolated from the expression system with 18 ± 1% active-site occupancy by NAD⁺ (HPLC) and 90 ± 1% active-site occupancy by NADH (fluorescence). Denaturation of the isolated enzyme yielded 24 ± 1% adenosine and 65 ± 1% adenine. Attempted reconstitution of apo-TcY435A with NAD⁺ or NADH yielded protein with no detectable occupancy.

Rate constants for dissociation of NAD⁺ from mutant SAHs HsY430A and TcY435A are 20-fold and 255-fold larger, respectively, than those for the corresponding wild-type enzymes—Cofactor dissociated from the mutant enzymes in

a simple first-order relaxation process (as previously observed in other cases [(7,9,17) and unpublished data of Q.-S. Li] in which the enzymic activity proceeded from full activity to zero activity). Mutant HsY430A released cofactor at 30 °C, pH 7.4, with $k_{\text{off}} = 4.2 \pm 0.1 \times 10^{-4} \text{ s}^{-1}$ while the wild-type enzyme Hs-SAHH released cofactor with $k_{\text{off}} = 1.9 \pm 0.3 \times 10^{-5} \text{ s}^{-1}$. The mutation therefore increases the dissociation rate constant by a factor of about 20. Mutant TcY435A released cofactor at 24 °C, pH 7.4, with $k_{\text{off}} = 2.8 \pm 0.2 \times 10^{-2} \text{ s}^{-1}$ while the wild-type enzyme Tc-SAHH released cofactor with $k_{\text{off}} = 1.1 \pm 0.2 \times 10^{-4} \text{ s}^{-1}$. The mutation therefore increases the dissociation rate constant by a factor of about 255. The values of these rate constants are included with other data in Table 2.

Association kinetics of NAD⁺ with mutant SAHs HsY430A and TcY435A—

These mutant enzymes exhibited (Supporting information) association time courses like those seen with the other SAHs [(7, 9, 17) and unpublished data of Q.-S. Li]: fast binding occurred within the dead-time of the experiment giving rise to an initial enzyme activity A_0 ; slow binding ensued with an apparent first-order rate constant k_{app} and combined with A_0 to give a final activity A_f . Each of these three parameters is a function of $[\text{NAD}^+]$. The expected dependences on the basis of a model to be described in the Discussion Section are given by eqs 1.

$$A_0 = (A_t/2) \{ [\text{NAD}^+]^n / (K_o^n + [\text{NAD}^+]^n) \} \quad (1a)$$

$$A_f = (A_t) \{ [\text{NAD}^+] / (K_f + [\text{NAD}^+]) \} \quad (1b)$$

$$k_{\text{app}} = k_a \{ [\text{NAD}^+] / (K_a + [\text{NAD}^+]) \} \quad (1c)$$

Here A_t is the total enzyme activity at saturating NAD^+ concentrations after completion of both phases of binding. Figure 2 shows (a) the dependences on $[\text{NAD}^+]$ of the fraction of fast binding A_0/A_t , the fraction of slow binding $(A_f - A_0)/A_t$, and the fraction of total binding A_f/A_t ; (b) the dependence of k_{app} on $[\text{NAD}^+]$ for the mutants HsY430A and TcY435A. The curves in Fig. 2 represent least-squares best fits of eqs 1 to the data, with parameters K_o , n , K_f , k_a , and K_a as given in Table 2.

Discussion

Computed free-energy contributions of individual residues to the cofactor affinities of Hs-SAHH and Tc-SAHH identify four conserved residues as the locus of differential cofactor affinities

The 38 residues within 5 Å of the NAD(H) binding site which may form strong interactions with cofactor NAD(H) were chosen for this study. The structures of Hs-SAHH and Tc-SAHH were overlaid and 34 out of the 38 residue pairs were found to be identical. The four pairs of non-identical residues were HsA219, TcC218; HsI244, TcV243; HsC278, TcN277; HsL417, TcI422, shown in boldface font in Table 1. None of these four non-identical residues, however, makes a significant free-energy contribution to the differential in the free energy of cofactor binding between Hs-SAHH and Tc-SAHH (Table 1). In fact, it is four pairs of *identical* residues (shown in red in Table 1: Hs/Tc N191/190; E243/242; K426/431; Y430/435) that show the most significant differential free-energy contributions (from about 3.4 to 7.4 kcal/mol) to the cofactor binding of Hs-SAHH and Tc-SAHH.

In deciding which cases to address experimentally, we took note of the facts that Turner et al. (18) had identified HsK426 and HsY430 as of special interest because they are “involved in interactions with the NAD bound predominantly to the other monomer,” an unusual feature of cofactor binding in SAHHs, and that Ault-Riché et al (19) had prepared the mutant HsK426A and found it to be devoid of cofactor affinity and catalytic activity. We therefore decided to concentrate on HsK426, HsY430, and the corresponding residues of Tc-SAHH, TcK431 and TcY435.

Y430 in the C-terminal extension of Hs-SAHH only slightly influences binding of NAD⁺ and NADH to apo-Hs-SAHH

The mutant HsY430A continues to bind NAD⁺ and NADH sufficiently strongly that the enzyme passes through the purification procedure from the expression system with essentially full occupancy of the cofactor sites ($116 \pm 7\%$). A preponderance of the cofactor sites was occupied by NADH ($86 \pm 5\%$). Denaturation resulted in release of a small amount of adenine (ca. 3%) and a larger amount ($81 \pm 1\%$) of adenosine. One possible explanation of these observations is that at least part of the NADH arose by oxidation of adenosine in the active site to 3'-ketoadenosine, which can decompose to generate adenine, the fragments then remaining in the active site in the “closed” conformation (1,6) of the enzyme. The isolated enzyme could be converted to the apo-enzyme and reconstituted to around 79% occupancy by NAD⁺, with the reconstituted enzyme exhibiting around 70% of the activity of wild-type enzyme which has full occupancy of NAD⁺. The HsY430A mutation thus has no large effect on the effective affinity of the enzyme for NAD⁺ or NADH, and little or no effect on the enzyme activity.

K431 in the C-terminal extension of Tc-SAHH is required for the binding of NAD⁺ and NADH to apo-Tc-SAHH

The mutant TcK431A is the equivalent of the mutant HsK426A, prepared in previous work (17) and shown to have lost both cofactor affinity and tetrameric structure. TcK431A maintains its tetrameric structure but is isolated from the expression system without cofactor and cannot be reconstituted under normal conditions with either NAD⁺ or NADH. Thus, as with Hs-SAHH, this lysine residue is critical for the cofactor affinity (it is thought to form hydrogen bonds to the 2'- or 3'-OH group of nicotinamide-bearing ribose ring) (1). It is striking that the mutation causes the loss of tetrameric structure in Hs-SAHH but not in Tc-SAHH. Previous comparisons [(7,17) and unpublished data of Dr. Li] of Hs-SAHH, Tc-SAHH, and their mutants have suggested that Hs-SAHH possesses a structure more robust with respect to mutation, typically showing smaller changes in its properties upon mutation than does Tc-SAHH. The quaternary structure would seem to be an exception to this rule.

Y435 in the C-terminal extension of Tc-SAHH is required for tight binding of NAD⁺ and NADH to apo-Tc-SAHH

The mutant TcY435A is the equivalent of HsY430A described above. Like HsY430A, the Tc-mutant is isolated with high occupancy of cofactor (mostly NADH) and releases a mixture of adenosine and adenine upon denaturation. Unlike HsY430A, the apo-form of the Tc-mutant no longer exhibits sufficient effective affinity for cofactor to permit reconstitution. The kinetic experiments reported here were conducted with enzyme as isolated from the expression system.

Rate constants for dissociation of NAD⁺ from mutant SAHs HsY430A and TcY435A are 20-fold and 255-fold larger, respectively, than those for the corresponding wild-type enzymes

The experimental results show that loss of the tyrosine in both enzymes increases the dissociation rate constant for NAD⁺, but not for NADH. The increase is an order of magnitude larger for the human than for the Tc-enzyme. This is consistent with the systematic observation cited above [(7,9,17) and unpublished data of Q.-S. Li] that the human enzyme is less susceptible to mutational changes in its properties than the trypanosomal enzyme.

Association kinetics of NAD⁺ with mutant SAHs HsY430A and TcY435A

Cofactor combination with these mutant enzymes followed a model previously observed with Hs-SAHH, Tc-SAHH and various mutants of both [(7,9,17) and unpublished data of Dr. Li]. The elements of this model are the following:

1. The apo-enzyme possesses two equally numbered classes of active sites.
2. Half of the sites are capable of binding cofactor rapidly (during the dead time of the experiment), with a relatively low affinity, and generating the full activity of these sites. This phenomenon accounts for the fast-binding activity A_0 observed at time zero from sites with cofactor-dissociation constant K_0 and Hill coefficient n .
3. Half of the apo-enzyme sites (slow-binding sites) are capable of binding cofactor rapidly, with a relatively high affinity (dissociation constant K_a), but initially generating no enzymic activity. These events initiate a time-dependent reorganization with rate constant k_a in which the slow-binding sites acquire full enzymic activity and all sites acquire a common cofactor-dissociation constant K_f , the final activity being A_f .

This model generates eqs 1 above, which were fit to the data as shown in Fig. 2, producing the values of K_0 , K_a , K_f , k_a , and n given in Table 2. Table 2 also gives these values for Hs-SAHH and Tc-SAHH as determined previously (7). Finally Table 2 presents values of the “on” rate constant for NAD⁺, estimated as described in the Materials and Methods section by two different methods, and the “off” rate constant for NAD⁺, obtained as described above. Together these allow the calculation of the equilibrium constant K_d for NAD⁺.

Comparison of the association kinetics for the wild-type enzymes Hs-SAHH and Tc-SAHH show no dramatic differences. The value of k_{off} is about 5-fold larger for Tc-SAHH and values for k_{on} smaller by 2 or 3-fold; the result is a dissociation constant 10 or 20-fold larger.

The mutant HsY430A has lower affinity for the fast-binding sites and a smaller reorganization rate constant k_a than Hs-SAHH, perhaps suggesting that some of the binding and reorganization events involve Y430 or its neighbors. The mutant off-rate is over 20-fold larger and the on-rate 4-fold slower than for Hs-SAHH, resulting in a dissociation constant larger by about 100-fold.

The mutant TcY435A exhibits far more dramatic effects: the constants K_0 , K_a , and K_f have all risen from the Tc-SAHH values of approximately micromolar values to around millimolar values, indicating that these affinities are significantly reduced by the removal of the tyrosine residue. The rate constant for reorganization is unaffected but the off-rate of cofactor is increased by nearly 1000-fold, while the on-rates are smaller by about 100-fold. The result is cofactor binding with a millimolar dissociation constant in the mutant to a sub-micromolar dissociation constant for the wild-type Tc-SAHH.

This relationship is similar to that for the HsY430A mutation and for the Tc-SAHH/Hs-SAHH comparison: a somewhat smaller decrease in on-rate combines with a larger increase in off-rate to generate a weaker cofactor binding in the mutant enzyme compared to the wild-type enzyme or in Tc-SAHH compared to Hs-SAHH.

Why do identical residues in two orthologous proteins give significantly different contributions to the binding free energy?

In the present study, the predicted differential contributions to the binding free energies of two pairs of identical amino acid residues have been largely confirmed by the experimental results, despite the intuitive notion that identical residues in two orthologous proteins should give similar binding free energy contributions. To investigate the reasons for this result, we examined the simulation snapshots of Tc-SAHH and Hs-SAHH. The C-loops of Hs-SAHH (in red) and Tc-SAHH (in blue) were superimposed and displayed, along with nearby NADHs, in Figure 3. We calculated the averages and standard errors of the distances of oxygen atoms of Lys or nitrogen atoms of Tyr to oxygen atoms of pyrophosphates between Tc-SAHH and Hs-SAHH. It is clear that these distances in Tc-SAHH and Hs-SAHH are different. Consequently the strength of the hydrogen bonds formed between Tyr or Lys and NADH is significantly different in these two enzymes. We rationalize that the distance difference between these C-loops and NADHs can be caused by the slightly different shape of the cofactor binding pocket or the overall conformation of the proteins, which originates from the sequence difference between these two proteins. Thus “identical” residues in two non-identical sequences should be regarded as only approximately identical.

Conclusion

Computational approaches and crystallographic structures of SAHHs suggest that a lysine residue and a tyrosine residue in a C-terminal extension of each subunit that forms part of the NAD⁺/NADH binding site in a partner subunit might be critical for full cofactor affinity. Earlier work (19) showed that the mutation HsK426A of the human enzyme Hs-SAHH eliminated both cofactor affinity and the tetrameric structure of the enzyme. Here we show that the corresponding mutation TcK431A in the trypanosomal enzyme Tc-SAHH greatly reduces cofactor affinity but leaves the tetrameric structure intact, a rare example in which the trypanosomal enzyme appears more robust to mutational damage than the human enzyme. Residue HsY430 modulates the association-dissociation kinetics significantly in the case of Hs-SAHH, generating through its mutation to Ala a decreased cofactor affinity by just under 100-fold. The corresponding mutation TcY435A decreased cofactor affinity by approximately 100,000-fold. Both effects arise from a larger increase in the off-rate of the cofactor, combined with a smaller decrease in on-rate. It should be noted that the values of K_f , the apparent dissociation constants of NAD⁺ corresponding to a period immediately after mixing of apoenzymes with cofactor, are on the order of micromolar for both Hs-SAHH and Tc-SAHH (Table 2). Binding at this level persists or strengthens by about 10-fold for Tc-SAHH but becomes stronger by about 100-fold for Hs-SAHH over a period of some hours, eventually reaching roughly nanomolar values of the dissociation constant (as reflected in the values of $k_{off}/(k_a/K_a)$ in Table 2). This phenomenon was observed previously (7) but remains unexplained.

These investigations demonstrate that free energy decomposition may be used to guide experimental studies by suggesting sensitive sites for mutagenesis. Our finding that identical residues in two orthologous proteins may give significantly different binding free energy contributions strongly suggests that comparative studies of homologous proteins should investigate not only different residues, but also identical residues in these proteins.

Supplementary Material

Refer to Web version on PubMed Central for supplementary material.

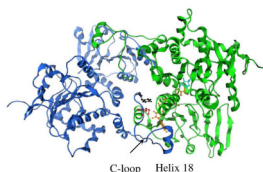
Abbreviations

2 x YT	2 x yeast extract tryptone
Ado	adenosine
AdoHcy	S-adenosyl-L-homocysteine
DTT	DL-Dithiothreitol
EDTA	ethylenediaminetetraacetic acid
FPLC	fast protein liquid chromatography
Hcy	L-homocysteine
HPLC	high performance liquid chromatography
Hs-SAHH	SAHH from <i>Homo sapiens</i> (human placenta)
NAD⁺	β -nicotinamide adenine dinucleotide
NADH	β -nicotinamide adenine dinucleotide, reduced form
<i>P. falciparum</i>	<i>Plasmodium falciparum</i>
SAHH	S-adenosyl-L-homocysteine hydrolase, EC 3.1.1.1
Tc-SAHH	SAHH from <i>Trypanosoma cruzi</i>
T. cruzi	<i>Trypanosoma cruzi</i>
rmsd	root-mean-square deviations
MM-GBSA	Molecular Mechanics-Generalized Born Surface Area
DHCeA	(1'R, 2'S, 3'R)-9-(2', 3'-dihydroxycyclopent-4'-enyl)adenine
NepA	neplanocin A

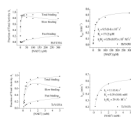
References

1. Turner MA, Yang X, Yin D, Kuczera K, Borchardt RT, Howell PL. Structure and function of S-adenosylhomocysteine hydrolase. *Cell Biochem Biophys.* 2000; 33:101–125. [PubMed: 11325033]
2. Parker NB, Yang X, Hanke J, Mason KA, Schowen RL, Borchardt RT, Yin DH. *Trypanosoma cruzi*: molecular cloning and characterization of the S-adenosylhomocysteine hydrolase. *Exp Parasitol.* 2003; 105:149–158. [PubMed: 14969692]
3. Creedon KA, Rathod PK, Wellems TE. *Plasmodium falciparum* S-adenosylhomocysteine hydrolase. cDNA identification, predicted protein sequence, and expression in *Escherichia coli*. *J Biol Chem.* 1994; 269:16364–16370. [PubMed: 8206944]
4. Yang X, Borchardt RT. Overexpression, purification, and characterization of S-adenosylhomocysteine hydrolase from *Leishmania donovani*. *Arch Biochem Biophys.* 2000; 383:272–280. [PubMed: 11185563]
5. Chiang PK. Biological effects of inhibitors of S-adenosylhomocysteine hydrolase. *Pharmacol Ther.* 1998; 77:115–134. [PubMed: 9578320]
6. Yang X, Hu Y, Yin DH, Turner MA, Wang M, Borchardt RT, Howell PL, Kuczera K, Schowen RL. Catalytic strategy of S-adenosyl-L-homocysteine hydrolase: transition-state stabilization and the avoidance of abortive reactions. *Biochemistry.* 2003; 42:1900–1909. [PubMed: 12590576]
7. Li QS, Cai S, Borchardt RT, Fang J, Kuczera K, Middaugh CR, Schowen RL. Comparative kinetics of cofactor association and dissociation for the human and trypanosomal s-adenosylhomocysteine

- hydrolases. 1. Basic features of the association and dissociation processes. *Biochemistry*. 2007; 46:5798–5809. [PubMed: 17447732]
8. Teixeira RA, Nitz N, Guimaro MC, Gomes C, Santos-Buch CA. Chagas disease. *Postgrad Med J*. 2006; 82:788–798. [PubMed: 17148699]
 9. Hu Y, Komoto J, Huang Y, Gomi T, Ogawa H, Takata Y, Fujioka M, Takusagawa F. Crystal structure of S-adenosylhomocysteine hydrolase from rat liver. *Biochemistry*. 1999; 38:8323–8333. [PubMed: 10387078]
 10. Kollman PA, Massova I, Reyes C, Kuhn B, Huo SH, Chong L, Lee M, Lee T, Duan Y, Wang W, Donini O, Cieplak P, Srinivasan J, Case DA, Cheatham TE. Calculating structures and free energies of complex molecules: Combining molecular mechanics and continuum models. *Accounts of Chemical Research*. 2000; 33:889–897. [PubMed: 11123888]
 11. Jorgensen WL, Chandrasekhar J, Madura JD, Impey RW, Klein ML. Comparison of simple potential functions for simulating liquid water. *J Chem Phys*. 1983; 79:926–935.
 12. Jakalian A, Bush BL, Jack DB, Bayly CI. Fast, efficient generation of high-quality atomic charges. AM1-BCC model: I. Method. *Journal of Computational Chemistry*. 2000; 21:132–146.
 13. Sugui C, Darden TA. Molecular dynamics simulations of biomolecules: long-range electrostatic effects. *Annu Rev Biophys Biomol Struct*. 1999; 28:155–179. [PubMed: 10410799]
 14. Miyamoto S, Kollman PA. Settle - an Analytical Version of the Shake and Rattle Algorithm for Rigid Water Models. *Journal of Computational Chemistry*. 1992; 13:952–962.
 15. Gohlke H, Kiel C, Case DA. Insights into protein-protein binding by binding free energy calculation and free energy decomposition for the Ras-Raf and Ras-RaIGDS complexes. *Journal of molecular biology*. 2003; 330:891–913. [PubMed: 12850155]
 16. Cai S, Li QS, Borchardt RT, Kuczera K, Schowen RL. The antiviral drug ribavirin is a selective inhibitor of S-adenosyl-L-homocysteine hydrolase from *Trypanosoma cruzi*. *Bioorg Med Chem*. 2007; 15:7281–7287. [PubMed: 17845853]
 17. Li QS, Cai S, Fang J, Borchardt RT, Kuczera K, Middaugh CR, Schowen RL. Comparative kinetics of cofactor association and dissociation for the human and trypanosomal S-adenosylhomocysteine hydrolases. 2. The role of helix 18 stability. *Biochemistry*. 2008; 47:4983–4991. [PubMed: 18393535]
 18. Turner MA, Yuan CS, Borchardt RT, Hershfield MS, Smith GD, Howell PL. Structure determination of selenomethionyl S-adenosylhomocysteine hydrolase using data at a single wavelength. *Nat Struct Biol*. 1998; 5:369–376. [PubMed: 9586999]
 19. Ault-Riche DB, Yuan CS, Borchardt RT. A single mutation at lysine 426 of human placental S-adenosylhomocysteine hydrolase inactivates the enzyme. *J Biol Chem*. 1994; 269:31472–31478. [PubMed: 7989313]

**Figure 1.**

The “dimer” structure of SAHHs that forms a part of the overall tetrameric enzyme structure (1). The monomers are shown in blue and green, with cofactor ligands in gold ball-and-stick representations and a substrate-analog ligand in a turquoise ball-and-stick representation. The C-terminal extension of each monomer, containing helix 18, can be seen penetrating into the partner monomer to form part of the cofactor binding site (top left, in green; bottom right, in blue). K426 (in red ball-and-stick) and Y430 (in black ball-and-stick) (Hs-SAHH) are located in the final coil between helix 18 and the C-terminus.

**Figure 2.**

Above: The fractions of fast binding, slow binding, and total binding of NAD^+ to the mutant enzyme HsY430A (left) and the value of the slow-binding rate constant k_{app} (right), both as a function of $[\text{NAD}^+]$. Below: The fractions of fast binding, slow binding, and total binding of NAD^+ to the mutant enzyme TcY435A (left) and the value of the slow-binding rate constant k_{app} (right), both as a function of $[\text{NAD}^+]$. The curves are drawn from eqs 1 with the least-squares best-fit parameters given in Table 2. Note that the concentration scales for HsY430A are below $300 \mu\text{M}$ while those for TcY435A go up to 5 mM .

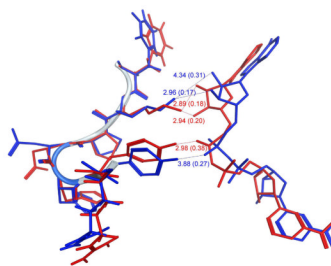


Figure 3. Superimposed C-loops of Hs-SAHH (in red) and Tc-SAHH (in blue) and nearby NADHs. The averages and standard errors of the distances of oxygen atoms of Lys and nitrogen atoms of Tyr to oxygen atoms of pyrophosphates are shown in either red (for Tc-SAHH) or blue (for Hs-SAHH).

Table 1

Contributions to the cofactor binding free energy of the 38 residues within 5 Å of the NAD(H) binding site in Hs-SAHH and Tc-SAHH. Units: kcal/mol. Four pairs of non-identical residues are shown in bold, while four pairs of residues are colored in red due to the significant difference in their free energy contribution.

Hs-SAHH Residues	157 THR	158 THR	159 THR	181 ASN	186 LYS	190 ASP	191 ASN	195 CYS	219 ALA	220 GLY
Free energy Contribution	-2.16	-6.26	-1.48	0.04	-0.72	0.1	-6.29	-0.6	-0.9	-1.55
Tc-SAHH Residues	156 THR	157 THR	158 THR	180 ASN	185 LYS	189 ASP	190 ASN	194 CYS	218 CYS	219 GLY
Free energy Contribution	-3	-6.88	-1.54	-0.29	-1.36	0.45	-1.55	-0.16	-0.86	-1.3
Hs-SAHH Residues	221 TYR	222 GLY	223 ASP	224 VAL	225 GLY	242 THR	243 GLU	244 ILE	245 ASP	248 ASN
Free energy Contribution	-1.44	-5.23	-0.36	-5.19	-0.51	-0.15	-3.3	-3.06	0.27	-1.19
Tc-SAHH Residues	220 TYR	221 GLY	222 ASP	223 VAL	224 GLY	241 THR	242 GLU	243 VAL	244 ASP	247 ASN
Free energy Contribution	-0.79	-3.61	0	-4.71	-0.12	-0.23	-9.68	-2.42	0.16	-0.11
Hs-SAHH Residues	275 THR	276 THR	277 GLY	278 CYS	281 ILE	299 ILE	300 GLY	301 HIS	305 GLU	344 LEU
Free energy Contribution	-0.26	-3.18	-0.27	-0.34	-1.23	-1.63	-1.41	-0.13	0.34	-0.6
Tc-SAHH Residues	274 THR	275 THR	276 GLY	277 ASN	280 ILE	298 ILE	299 GLY	300 HIS	304 GLU	343 LEU
Free energy Contribution	-0.13	-3.56	-0.96	-0.67	-0.98	-1.85	-1.09	-1.96	0.5	-0.52
Hs-SAHH Residues	346 ASN	353 HIS	407* THR	409* LEU	413* GLN	417* LEU	426* LYS	430* TYR		
Free energy Contribution	-2.84	-0.46	-0.99	-0.63	0.02	-0.17	-10.01	-3.87		
Tc-SAHH Residues	344 ASN	352 HIS	412* THR	414* LEU	418* GLN	422* ILE	431* LYS	435* TYR		
Free energy Contribution	-2.08	0.06	-0.58	-0.19	0.12	-1.06	-2.65	-0.49		

* These residues are from the tail of the second chain.

Table 2

Values of rate and equilibrium constants for the kinetics of the fast and slow binding phases of the association reaction of NAD⁺ with Hs-SAHH, HsY430A, Tc-SAHH, and TcY435A at 23 °C and pH 7.4, from reference (7,17) and from fits of the data in Fig. 2 to eqs. 1.

Enzyme	K_{on} , μM binding to fully functional sites of apo-SAHH	K_{ap} , μM binding to non-functional sites of apo-SAHH	K_f , μM binding to fully functional sites of holo-SAHH	$10^3 k_{sp}$, s^{-1} transformation of non-functional apo-sites to functional holo-sites	$10^{-3} k_d/K_{ap}$, $\text{M}^{-1}\text{s}^{-1}$ binding and transformation of apo-sites to holo-sites	$10^{-3} k_{on}$, $\text{M}^{-1}\text{s}^{-1}$	$10^6 k_{off}$, s^{-1}	K_{d0} , nM
	k_{off}/k_{on} $k_{off}/(k_{sp}/K_{ap})$							
Hs-SAHH	33 ± 4 $n = 3.3 \pm 1.4$	19 ± 8	1.4 ± 0.3	55 ± 8	2.9 ± 1.2	1.9 ± 0.04	19 ± 3	10 ± 2 7 ± 3
HsY430A	432 ± 93 $n = 0.9 \pm 0.1$	17 ± 2	2.0 ± 0.3	9.5 ± 0.4	0.56 ± 0.07	0.54 ± 0.04	420 ± 10	784 ± 64 750 ± 95
Tc-SAHH	38 ± 9 $n = 1.6 \pm 0.4$	3.8 ± 0.6	1.8 ± 0.4	6.0 ± 0.2	1.6 ± 0.3	0.68 ± 0.02	110 ± 20	161 ± 30 69 ± 18
	K_{on} , mM	K_{ap} , mM	K_f , mM	k_{sp} , s^{-1}	k_d/K_{ap} , $\text{M}^{-1}\text{s}^{-1}$	k_{on} , $\text{M}^{-1}\text{s}^{-1}$	$10^3 k_{off}$, s^{-1}	K_{d0} , mM
TcY435A	2.6 ± 1 $n = 0.6 \pm 0.2$	0.39 ± 0.04	0.20 ± 0.03	11 ± 0.4	29 ± 9	18 ± 2	28 ± 2	1.6 ± 0.2 1.0 ± 0.3